

## Pyroeffects on magneto-electro-elastic sensor bonded on mild steel cylindrical shell

P. Kondaiah<sup>\*1</sup>, K. Shankar<sup>2a</sup> and N. Ganesan<sup>2b</sup>

<sup>1</sup>Department of Mechanical Engineering, School of Engineering & Technology, Mahindra École Centrale, Hyderabad, Andhra Pradesh 500043, India

<sup>2</sup>Machine Design Section, Department of Mechanical Engineering, Indian Institute of Technology Madras, Chennai 600036, India

(Received June 6, 2014, Revised January 19, 2015, Accepted January 23, 2015)

**Abstract.** Magneto-electro-elastic (MEE) materials under thermal environment exhibits pyroelectric and pyromagnetic coefficients resulting in pyroeffects such as pyroelectric and pyromagnetic. The pyroeffects on the behavior of multiphase MEE sensor bonded on top surface of a mild steel cylindrical shell under thermal environment is presented in this paper. The study aims to investigate how samples having different volume fractions of the multiphase MEE sensor behave due to pyroeffects using semi-analytical finite element method. This is studied at an optimal location on a mild steel cylindrical shell, where the maximum electric and magnetic potentials are induced due to these pyroeffects under different boundary conditions. It is assumed that sensor and shell is perfectly bonded to each other. The maximum pyroeffects on electric and magnetic potentials are observed when volume fraction is  $v_f = 0.2$ . Additionally, the boundary conditions significantly influence the pyroeffects on electric and magnetic potentials.

**Keywords:** pyroelectric; pyromagnetic; magneto-electro-elastic sensor; cylindrical shell; semi-analytical finite element

### 1. Introduction

Magneto-Electro-Elastic (MEE) composite materials have the ability to generate magnetic, electric and mechanical responses when they experience a thermal stimulus due to its significant coupling between mechanical, electric, magnetic and thermal fields, which are potentially useful in smart or intelligent structure applications. MEE material exhibits magnetic-electric-mechanical coupling effect in such a way that they produce electric and magnetic fields when deformed and conversely, undergo deformation when subjected to electric and magnetic field. The magnetoelectric coupling effect which is absent in the constituent components is exhibited by this class of material. In addition to this, the pyroelectric and pyromagnetic coupling effects which are present with a thermal field are also exhibited by this class of MEE materials. This cross or product property is created by coupling of elastic deformations in the piezoelectric and

---

\*Corresponding author, Assistant Professor, E-mail: [kondaiah.iitm@gmail.com](mailto:kondaiah.iitm@gmail.com)

<sup>a</sup>Professor, E-mail: [skris@iitm.ac.in](mailto:skris@iitm.ac.in)

<sup>b</sup>Professor Emeritus, E-mail: [nganesan@iitm.ac.in](mailto:nganesan@iitm.ac.in)

piezomagnetic phases and the elastic deformations may be induced directly by mechanical loading/temperature gradient or indirectly by an application of electric or magnetic field. This unique feature allows magnetic control of electric polarization, electric control of magnetization and control of electric and magnetic fields with mechanical stress. Due to the exceptional nature of these materials to convert one form of energy into another, find widespread applications in areas like magnetic field probes, acoustic devices, medical ultrasonic imaging, sensors and actuators Wu and Huang (2000).

Aboudi (2001) has presented the effective moduli of magneto-electro-elastic composite by employing homogenization method with the assumption that composites have a periodic structure. Sunar *et al.* (2002) has presented finite element modeling of a fully coupled thermopiezomagnetic continuum with the aid of thermodynamic potential. Sirohi *et al.* (2000) investigated the piezoceramic (PZT) strain sensors by measuring the strain generated by direct piezoelectric effect. Mahieddine and Ouali (2008) have used finite element model to analyze beams with piezoelectric sensors and actuators based on first order Kirchoff theory. Various parametric studies were conducted to demonstrate the application of piezoelectric effect in active vibration control. Daga *et al.* (2009) has presented the transient sensory response of magneto-electro-elastic composite containing different volume fractions of Barium Titanate in a matrix of Cobalt Iron Oxide by using magnetic scalar potential approach.

Soh and Liu (2005) has presented the recent research advances on the magnetolectric coupling effect of piezoelectric-piezomagnetic composite materials and their fundamental mechanics issues are reviewed comprehensively. The eight sets of constitutive equations for magneto-electro-elastic solids and the energy functions corresponding to each set of constitutive equations are given. The mathematical properties of the thermodynamic potentials and the relations between the material constants are discussed. Ryu *et al.* (2002) investigated ME particulate composites and laminate composites and summarized the important results. They concluded that to obtain excellent ME property from the ME laminate composites, a high piezoelectric voltage coefficient, an optimum thickness ratio between piezoelectric layer and Terfenol-D layers, the direction of magnetostriction in the Terfenol-D disks, and higher elastic compliance of piezoelectric material were important factors. Nan *et al.* (2008) studied bulk and nanostructured multiferroic MEE composite consisting of ferroelectric and magnetic phases in experimental and theoretical perspectives. The effects of geometric size and mechanical boundary conditions on bilayered composites for magneto-electric coupling was investigated by Pan *et al.* (2009) using three dimensional finite element approach. The theoretical analysis of a multilayered magneto-electro-thermoelastic hollow cylinder under unsteady and uniform surface heating is presented by Ootao and Ishihara (2011). The exact solution of transient thermal stress problem with the assumption of plane strain state is obtained. Additionally without considering the pyroelectric and pyromagnetic effects, investigated the effects of coupling between magnetic, electric and thermoelastic fields. Guiffard *et al.* (2010) were studied room temperature magnetic field detection using single piezoelectric disk with a good sensitivity and linear response versus dc magnetic field change. This study validates that ME effect originates from the presence of eddy currents within the metal electrodes of the ceramic, thus yielding radial Lorentz stress which is transduced to the PZT. Kalamkarov *et al.* (2009) have presented the new trends in application of asymptotic homogenization techniques to the analysis of composite materials and thin-walled composite structures and their effective properties. In addition to review the existing results, they introduced a possibility of analytical solution of the unit cell problems obtained as a result of the homogenization procedure. Kalamkarov (2014) has developed micromechanical models by applying asymptotic homogenization technique and obtained

analytical formulae for the effective properties to composite materials and thin-walled composite structures.

Recently, Hadjiloizi *et al.* (2013a) and Hadjiloizi *et al.* (2013b) have presented the effective pyroelectric and pyromagnetic coefficients in micromechanical analysis of magneto-electro-thermo-elastic composite for quasi-static model using the asymptotic homogenization method. The results of this model fully agree with Bravo-Castillero *et al.* (2008). Study of these pyroelectric and pyromagnetic coefficients resulting in pyroelectric and pyromagnetic effects on MEE sensor to account the thermal environment for enhancing the performance of the sensor was uncovered till date. Hence the present work is attempted.

## 2. Theoretical formulation

### 2.1 Constitutive equations

In a cylindrical coordinate system  $(r, \theta, z)$ , the coupled constitutive equations for linearly magneto-electro-elastic three dimensional solid under thermal environment (where thermal field is not fully coupled with the magneto-electro-elastic field) can be written as (Gao and Noda 2004, Ganesan *et al.* 2007)

$$\left. \begin{aligned} \sigma_j &= c_{jk} S_k - e_{mj} E_m - q_{mj} H_m - \gamma_j \Theta \\ D_l &= e_{lk} S_k + \varepsilon_{lm} E_m + m_{lm} H_m + p_l \Theta \\ B_l &= q_{lk} S_k + m_{lm} E_m + \mu_{lm} H_m + \tau_l \Theta \end{aligned} \right\} \quad (1)$$

where  $c_{jk}$ ,  $e_{lk}$ ,  $q_{lk}$  are elastic, piezoelectric, piezomagnetic, stress-temperature coefficients respectively and  $\gamma_j$  is the thermal stress coefficient being related with the thermal expansion coefficient  $\beta$  by  $\gamma = c\beta$ .  $\varepsilon_{lm}$ ,  $m_{lm}$ ,  $\mu_{lm}$ ,  $p_l$  and  $\tau_l$  represents respectively the dielectric, magneto-electric, magnetic permeability, pyroelectric and pyromagnetic tensors. These equations relate stress ( $\sigma_j$ ), electric displacement ( $D_l$ ) and magnetic flux density ( $B_l$ ) to strain ( $S_k$ ), electric field ( $E_m$ ), magnetic field ( $H_m$ ) and temperature rise ( $\Theta$ ).

### 2.2 Semi-analytical finite element formulation

The semi-analytical finite element formulation discussed in this section pertains to an axisymmetric shell subjected to arbitrary temperature along the circumferential ( $\theta$ ) direction of the shell. In addition, the arbitrary temperature distribution can be expanded using Fourier series in circumferential direction. Even though the derivation here is given in general as the shell is subjected to constant temperature in the circumferential direction. For an axisymmetric cylindrical shell, the geometry and material properties does not vary in the circumferential ( $\theta$ ) direction and semi-analytical finite element approach can be used for a simplified solution. For a general case the thermal displacements, electric potential and magnetic potential are expressed using Fourier series in circumferential direction as

$$\left. \begin{aligned} u_r &= \sum u_r(r, z) \cos n\theta \\ u_\theta &= \sum u_\theta(r, z) \sin n\theta \\ u_z &= \sum u_z(r, z) \cos n\theta \\ \phi &= \sum \phi(r, z) \cos n\theta \\ \psi &= \sum \psi(r, z) \cos n\theta \end{aligned} \right\} \quad (2)$$

Solution corresponding to  $n = 0$  pertains to an axisymmetric problem. The analysis has been reduced for finite element in radial ( $r$ ) and axial ( $z$ ) directions.  $u_r$ ,  $u_\theta$  and  $u_z$  are the radial, circumferential and axial displacements respectively,  $\phi$  is the electric potential and  $\psi$  is the magnetic potential.  $u_r(r, z)$ ,  $u_\theta(r, z)$ ,  $u_z(r, z)$ ,  $\phi(r, z)$ ,  $\psi(r, z)$  are the amplitudes of the symmetric components of the primary variables. The semi-analytical finite element formulation of the coupled magneto-electro-elastic problem is derived by approximating the displacement ( $\{u\} = \{u_r, u_\theta, u_z\}^T$ ), electric potential ( $\phi$ ), and magnetic potential ( $\psi$ ) on element level using suitable shape functions and corresponding nodal quantities as

$$\left. \begin{aligned} u &= [N_u(r, z)] \{u^e\} \\ \phi &= [N_\phi(r, z)] \{\phi^e\} \\ \psi &= [N_\psi(r, z)] \{\psi^e\} \end{aligned} \right\} \quad (3)$$

where  $N_u$ ,  $N_\phi$  and  $N_\psi$  are shape functions for mechanical, electrical, and magnetic fields respectively. Using the semi-analytical finite element approach, the shell geometry is modelled with four-noded isoparametric element having shape functions

$$N_i(\xi, \eta) = \frac{1}{4}(1 + \xi\xi_i)(1 + \eta\eta_i) \quad \text{for } i = 1, 2, 3, 4$$

where  $\xi$  and  $\eta$  are the natural coordinates.

The strain-displacement, electric field-electric potential and magnetic field-magnetic potential are used in the finite element analysis along with the constitutive Eq. (1). In cylindrical coordinates, the strain-displacement relation can be written as

$$\left. \begin{aligned} S_{rr} &= \frac{\partial u_r}{\partial r}, \quad S_{\theta\theta} = \frac{1}{r} \left( \frac{\partial u_\theta}{\partial \theta} + u_r \right), \\ S_{zz} &= \frac{\partial u_z}{\partial z}, \quad S_{\theta z} = \frac{\partial u_\theta}{\partial z} + \frac{1}{r} \frac{\partial u_z}{\partial \theta}, \\ S_{rz} &= \frac{\partial u_z}{\partial r} + \frac{\partial u_r}{\partial z}, \quad S_{r\theta} = \frac{1}{r} \frac{\partial u_r}{\partial \theta} + \frac{\partial u_\theta}{\partial r} - \frac{u_\theta}{r} \end{aligned} \right\} \quad (4)$$

where  $S_{ij}$  is strain component. The angular displacements are absent in axisymmetric problem, hence the derivatives of all parameters with respect to  $\theta$  are equal to zero. So the strain-displacement relations are re-written as

$$S_{rr} = \frac{\partial u_r}{\partial r}, \quad S_{\theta\theta} = \frac{u_r}{r}, \quad S_{zz} = \frac{\partial u_z}{\partial z}, \quad S_{rz} = \frac{\partial u_z}{\partial r} + \frac{\partial u_r}{\partial z}, \quad S_{r\theta} = 0 \quad S_{\theta z} = 0 \quad (5)$$

For obtaining the element level governing equations for strain (S), the strain vector within element can be expressed in terms of derivatives of shape functions and nodal quantities as

$$\{S\} = [B_u] \{u^e\} \quad (6)$$

where  $[B_u]$ , the strain displacement matrix, can be written as

$$[B_u] = [L_u][N_u] = \begin{bmatrix} \frac{\partial}{\partial r} & 0 & 0 \\ \frac{1}{r} & \frac{1}{r} \frac{\partial}{\partial \theta} & 0 \\ 0 & 0 & \frac{\partial}{\partial z} \\ 0 & \frac{\partial}{\partial z} & \frac{1}{r} \frac{\partial}{\partial \theta} \\ \frac{\partial}{\partial z} & 0 & \frac{\partial}{\partial r} \\ \frac{1}{r} \frac{\partial}{\partial \theta} & \frac{\partial}{\partial r} - \frac{1}{r} & 0 \end{bmatrix} \times \begin{bmatrix} N_1 & 0 & 0 & N_2 & 0 & 0 & N_3 & 0 & 0 & N_4 & 0 & 0 \\ 0 & N_1 & 0 & 0 & N_2 & 0 & 0 & N_3 & 0 & 0 & N_4 & 0 \\ 0 & 0 & N_1 & 0 & 0 & N_2 & 0 & 0 & N_3 & 0 & 0 & N_4 \end{bmatrix}$$

$$\Rightarrow [B_u] = \begin{bmatrix} \frac{\partial N_u}{\partial r} & 0 & 0 \\ \frac{N_u}{r} & \frac{nN_u}{r} & 0 \\ 0 & 0 & \frac{\partial N_u}{\partial z} \\ 0 & \frac{\partial N_u}{\partial z} & -\frac{nN_u}{r} \\ \frac{\partial N_u}{\partial z} & 0 & \frac{\partial N_u}{\partial r} \\ -\frac{nN_u}{r} & \frac{\partial N_u}{\partial r} - \frac{N_u}{r} & 0 \end{bmatrix} \quad \text{for } u = 1, 2, \dots, 4$$

Similarly, the relation between electric field (E) and electric potential ( $\phi$ ); magnetic field (H) and magnetic potential ( $\psi$ ) can be written as

$$E_r = -\frac{\partial \phi}{\partial r}, \quad E_\theta = -\frac{1}{r} \frac{\partial \phi}{\partial \theta}, \quad E_z = -\frac{\partial \phi}{\partial z} \quad (7)$$

$$H_r = -\frac{\partial \psi}{\partial r}, \quad H_\theta = -\frac{1}{r} \frac{\partial \psi}{\partial \theta}, \quad H_z = -\frac{\partial \psi}{\partial z} \quad (8)$$

The electric and magnetic field vectors within element can be expressed in terms of respective derivatives of shape functions and nodal quantities to get element level governing equations as

$$\{E\} = [B_\phi] \{\phi^e\} \tag{9}$$

$$\{H\} = [B_\psi] \{\psi^e\} \tag{10}$$

where  $[B_\phi]$  and  $[B_\psi]$  are the derivative of shape function matrices, can be written as

$$[B_\phi] = [B_\psi] = [L_i][N_i] \Rightarrow \begin{bmatrix} -\frac{\partial}{\partial r} \\ -\frac{1}{r} \frac{\partial}{\partial \theta} \\ -\frac{\partial}{\partial z} \end{bmatrix} [N_1 \quad N_2 \quad N_3 \quad N_4] \quad \text{for } i = \phi, \psi$$

$$\Rightarrow \begin{bmatrix} -\frac{\partial N_1}{\partial r} & -\frac{\partial N_2}{\partial r} & -\frac{\partial N_3}{\partial r} & -\frac{\partial N_4}{\partial r} \\ \frac{nN_1}{r} & \frac{nN_2}{r} & \frac{nN_3}{r} & \frac{nN_4}{r} \\ -\frac{\partial N_1}{\partial z} & -\frac{\partial N_2}{\partial z} & -\frac{\partial N_3}{\partial z} & -\frac{\partial N_4}{\partial z} \end{bmatrix}$$

The derivation of finite element equations for magneto-electro-thermo-elastic material by considering body force, traction and heat flux using virtual displacement principle is given by Ganesan *et al.* (2007) and it is written as

$$\begin{aligned} [M_{uu}^e] \{\ddot{u}^e\} - [C_{u\Theta}^e] \{\dot{\Theta}^e\} + [K_{uu}^e] \{u^e\} + [K_{u\phi}^e] \{\phi^e\} + [K_{u\psi}^e] \{\psi^e\} - [K_{u\Theta}^e] \{\Theta^e\} &= \{f_u^e\} + \{T_u^e\} \\ [K_{u\phi}^e]^T \{u^e\} - [K_{\phi\phi}^e] \{\phi^e\} - [K_{\phi\psi}^e] \{\psi^e\} + [K_{\phi\Theta}^e] \{\Theta^e\} &= 0 \\ [K_{u\psi}^e]^T \{u^e\} - [K_{\psi\psi}^e] \{\psi^e\} - [K_{\psi\Theta}^e] \{\Theta^e\} &= 0 \\ [C_{\Theta u}^e]^T \{\dot{u}^e\} - [C_{\Theta\phi}^e] \{\dot{\phi}^e\} - [C_{\Theta\psi}^e] \{\dot{\psi}^e\} + [C_{\Theta\Theta}^e] \{\dot{\Theta}^e\} + [K_{\Theta\Theta}^e] \{\Theta^e\} &= -\{T_\Theta^e\} \end{aligned} \tag{11}$$

The above equation can be expressed in matrix form as

$$\begin{bmatrix} M_{uu}^e & 0 & 0 & 0 \\ 0 & 0 & 0 & 0 \\ 0 & 0 & 0 & 0 \\ 0 & 0 & 0 & 0 \end{bmatrix} \begin{Bmatrix} \ddot{u}^e \\ \ddot{\phi}^e \\ \ddot{\psi}^e \\ \dot{\Theta}^e \end{Bmatrix} + \begin{bmatrix} 0 & 0 & 0 & -C_{u\Theta}^e \\ 0 & 0 & 0 & 0 \\ 0 & 0 & 0 & 0 \\ C_{\Theta u}^e & -C_{\Theta\phi}^e & -C_{\Theta\psi}^e & C_{\Theta\Theta}^e \end{bmatrix} \begin{Bmatrix} \dot{u}^e \\ \dot{\phi}^e \\ \dot{\psi}^e \\ \dot{\Theta}^e \end{Bmatrix} + \begin{bmatrix} K_{uu}^e & K_{u\phi}^e & K_{u\psi}^e & -K_{u\Theta}^e \\ K_{\phi u}^e & -K_{\phi\phi}^e & -K_{\phi\psi}^e & K_{\phi\Theta}^e \\ K_{\psi u}^e & -K_{\psi\phi}^e & -K_{\psi\psi}^e & K_{\psi\Theta}^e \\ 0 & 0 & 0 & K_{\Theta\Theta}^e \end{bmatrix} \begin{Bmatrix} u^e \\ \phi^e \\ \psi^e \\ \Theta^e \end{Bmatrix} = \begin{Bmatrix} f_u^e + T_u^e \\ 0 \\ 0 \\ -T_\Theta^e \end{Bmatrix} \tag{12}$$

From Eq. (12), assembling all element contributions, the equation of motion can be written as

$$[M]\{\ddot{v}\} + [D]\{\dot{v}\} + [K]\{v\} = \{F\} \tag{13}$$

where

$$[M] = \begin{bmatrix} M_{uu}^e & 0 & 0 & 0 \\ 0 & 0 & 0 & 0 \\ 0 & 0 & 0 & 0 \\ 0 & 0 & 0 & 0 \end{bmatrix}; [D] = \begin{bmatrix} 0 & 0 & 0 & -C_{u\Theta}^e \\ 0 & 0 & 0 & 0 \\ 0 & 0 & 0 & 0 \\ C_{\Theta u}^e & -C_{\Theta\phi}^e & -C_{\Theta\psi}^e & C_{\Theta\Theta}^e \end{bmatrix};$$

$$[K] = \begin{bmatrix} K_{uu}^e & K_{u\phi}^e & K_{u\psi}^e & -K_{u\Theta}^e \\ K_{\phi u}^e & -K_{\phi\phi}^e & -K_{\phi\psi}^e & K_{\phi\Theta}^e \\ K_{\psi u}^e & -K_{\psi\phi}^e & -K_{\psi\psi}^e & K_{\psi\Theta}^e \\ 0 & 0 & 0 & K_{\Theta\Theta}^e \end{bmatrix};$$

$$\{F\} = \begin{Bmatrix} f_u^e + T_u^e \\ 0 \\ 0 \\ -T_{\Theta}^e \end{Bmatrix}; \{v\} = \begin{Bmatrix} u^e \\ \phi^e \\ \psi^e \\ \Theta^e \end{Bmatrix}$$

Eq. (13) can be used to investigate the dynamic behavior of the magneto-electro-thermo-elastic material where the mechanical, electrical, magnetic and thermal fields are fully coupled. To investigate the pyroelectric and pyromagnetic effects on behavior of multiphase magneto-electro-elastic cylindrical shell, the above equation is reduced to static case along with the following assumptions,

1. Thermal field of the system is uniform and not fully coupled with the magneto-electro-elastic field, i.e., the magneto-electro-elastic field can be affected by the temperature field through constitutive relations but the temperature field is not affected by the magneto-electro-elastic field.
2. The mechanical, electric and magnetic fields are fully coupled.
3. The externally applied mechanical force, electric charge and magnetic current are assumed to be zero.

Based on the above assumptions, Eq. (13) can be written as

$$\left. \begin{aligned} [K_{uu}^e]\{u^e\} + [K_{u\phi}^e]\{\phi^e\} + [K_{u\psi}^e]\{\psi^e\} &= \{F_u^e + F_{u\Theta}^e\} \\ [K_{u\phi}^e]^T\{u^e\} - [K_{\phi\phi}^e]\{\phi^e\} - [K_{\phi\psi}^e]\{\psi^e\} &= \{F_{\phi}^e - F_{\phi\Theta}^e\} \\ [K_{u\psi}^e]^T\{u^e\} - [K_{\phi\psi}^e]^T\{\phi^e\} - [K_{\psi\psi}^e]\{\psi^e\} &= \{F_{\psi}^e - F_{\psi\Theta}^e\} \end{aligned} \right\} \tag{14}$$

where  $\{F_u^e\}$ ,  $\{F_{\phi}^e\}$  and  $\{F_{\psi}^e\}$  corresponds to externally applied mechanical force, electric charge and magnetic current vectors respectively.  $\{F_{u\Theta}^e\}$ ,  $\{F_{\phi\Theta}^e\}$  and  $\{F_{\psi\Theta}^e\}$  represents respectively the thermal, pyroelectric and pyromagnetic load vectors. (Note: The negative signs of  $\{F_{\phi\Theta}^e\}$  and

$\{F_{\psi\Theta}^e\}$  in Eq. (14) are taken care of by pyroelectric and pyromagnetic properties in Table 1). Without considering the applied  $\{F_u^e\}$ ,  $\{F_\phi^e\}$  and  $\{F_\psi^e\}$  load vectors, Eq. (14) can be written as

$$\left. \begin{aligned} [K_{uu}^e] \{u^e\} + [K_{u\phi}^e] \{\phi^e\} + [K_{u\psi}^e] \{\psi^e\} &= \{F_{u\Theta}^e\} \\ [K_{u\phi}^e]^T \{u^e\} - [K_{\phi\phi}^e] \{\phi^e\} - [K_{\phi\psi}^e] \{\psi^e\} &= \{F_{\phi\Theta}^e\} \\ [K_{u\psi}^e]^T \{u^e\} - [K_{\phi\psi}^e]^T \{\phi^e\} - [K_{\psi\psi}^e] \{\psi^e\} &= \{F_{\psi\Theta}^e\} \end{aligned} \right\} \quad (15)$$

where, the matrix  $K_{u\phi}$  is stiffness matrix due to piezoelectric-mechanical coupling effect, and  $K_{u\psi}$  is stiffness matrix due to piezomagnetic-mechanical coupling effect, and  $K_{\phi\psi}$  is stiffness matrix due to magneto-electric coupling effect.  $K_{u\Theta}$ ,  $K_{\phi\Theta}$  and  $K_{\psi\Theta}$  are stiffness matrices due to thermal-mechanical, thermal-electrical and thermal-magnetic coupling effects respectively. The matrices  $K_{uu}$ ,  $K_{\phi\phi}$  and  $K_{\psi\psi}$  are stiffness matrices due to mechanical, electrical and magnetic fields respectively.

### 2.2.1 Evaluation of elemental matrices

The different elemental stiffness matrices of Eq. (15) for magneto-electro-elastic cylindrical shell are further defined as

$$\begin{aligned} [K_{uu}^e] &= \int_v [B_u]^T [c] [B_u] dv; \quad [K_{u\phi}^e] = \int_v [B_u]^T [e] [B_\phi] dv; \quad [K_{u\psi}^e] = \int_v [B_u]^T [q] [B_\psi] dv; \\ [K_{\phi\psi}^e] &= \int_v [B_\phi]^T [m] [B_\psi] dv; \quad [K_{\phi\phi}^e] = \int_v [B_\phi]^T [\varepsilon] [B_\phi] dv; \quad [K_{\psi\psi}^e] = \int_v [B_\psi]^T [\mu] [B_\psi] dv \end{aligned}$$

The volume integration is replaced with  $dv = 2\pi r dr dz$  for axisymmetric problems. In the present study, axisymmetric temperature is considered to be the known quantity and hence the thermal load term, and pyroelectric load (electric load generated due to axisymmetric temperature) and pyromagnetic load (magnetic load generated due to axisymmetric temperature) terms can be treated as external loadings in the system equations. These can be solved for displacements, electric potential and magnetic potential. These external vectors used in the system equations are given as follows

$$\{F_{u\Theta}^e\} = [K_{u\Theta}^e] \{\Theta\} = \int_v [B_u]^T [c] [\beta] \Theta dv \quad (16)$$

where  $\{F_{u\Theta}^e\}$  is the thermal load vector and is governed as a direct effect on displacements, and indirect effect on electric and magnetic potentials through constitutive equations.

$$\{F_{\phi\Theta}^e\} = [K_{\phi\Theta}^e] \{\Theta\} = \int_v [B_\phi]^T [p] \Theta dv \quad (17)$$

where  $\{F_{\phi\Theta}^e\}$  is the pyroelectric load vector and is governed as a direct effect on electric potential, and indirect effect on magnetic potential and displacement through constitutive equations.

$$\{F_{\psi\Theta}^e\} = [K_{\psi\Theta}^e] \{\Theta\} = \int_v [B_\psi]^T [\tau] \Theta dv \quad (18)$$

where  $\{F_{\psi\Theta}^e\}$  is the pyromagnetic load vector and it is governed as a direct effect on magnetic

potential, and indirect effect on electric potential and displacements through constitutive equations. The coupled formation of Eq. (15) can be written as

$$\begin{bmatrix} K_{uu} & K_{u\phi} & K_{u\psi} \\ K_{\phi u} & -K_{\phi\phi} & -K_{\phi\psi} \\ K_{\psi u} & -K_{\psi\phi} & -K_{\psi\psi} \end{bmatrix} \begin{Bmatrix} u \\ \phi \\ \psi \end{Bmatrix} = \begin{Bmatrix} F_{u\Theta} \\ F_{\phi\Theta} \\ F_{\psi\Theta} \end{Bmatrix} \quad (19)$$

### 3. Results and discussion

The semi-analytical finite element method is used to analyze pyroeffects on behavior of magneto-electro-elastic sensor bonded on top surface of a mild steel cylindrical shell subjected to uniform temperature rise of 50 K. The purpose of the sensor is to measure electric and magnetic response to applied thermal environment. The main objective of the present work is to find out how samples having different volume fractions of the multiphase MEE sensor behave due to pyroeffects using semi-analytical finite element method. The sensor bonded on top surface of the cylindrical shell at optimal location (clamped end) is considered based on optimal sensor placement as discussed in Section 3.2. The advantage of considering optimal sensor placement study is that there is no need to analyze the sensor behavior at selective locations such as clamped end, intermediate location, free end, etc. The multiphase magneto-electro-elastic cylindrical shell is made of piezomagnetic (CoFe<sub>2</sub>O<sub>4</sub>) matrix reinforced by piezoelectric (BaTiO<sub>3</sub>) material for different volume fractions from  $v_f = 0$  to 1. The  $v_f = 1.0$  corresponds to pure piezoelectric material and  $v_f = 0.0$  corresponds to pure piezomagnetic material.

The multiphase MEE cylindrical shell is analyzed with uniform axisymmetric temperature to study the pyroeffects under clamped-clamped and clamped-free boundary conditions. The pyroelectric effect can manifest through the pyroelectric loading term given in Eq. (17). The pyromagnetic effect can manifest through the pyromagnetic loading term given in Eq. (18). Influence of these two (pyroelectric and pyromagnetic loads) are called direct effect on electric and magnetic potentials. In contrast, due to thermal loading (Refer Eq. (16)) also electric and magnetic potential can be developed through constitutive equations. This is called indirect effect on electric and magnetic potentials (Refer Section 2.2.1). Whereas in the case of displacement, it is vice-versa.

The sensor is bonded at an optimal location (clamped end) on outer surface of the shell under both clamped-free and clamped-clamped boundary conditions. It is assumed that the mild steel shell and the sensor are perfectly bonded to each other. Semi-analytical finite element method is used to model the structure. Fig. 1 schematically represents the mild steel cylinder with sensor patch bonded at optimal location on its outer surface. The dimensions of axisymmetric cylindrical shell used for analysis are as follows: length of the cylinder ( $l$ ) = 4.0 m, inner radius ( $r_i$ ) = 0.995 m and thickness of the cylinder ( $t$ ) = 0.01 m. The material properties are given in Table 1. The displacement, electric and magnetic potentials of the sensor are considered in the present analysis under both boundary conditions. To study the pyroeffects on bonded MEE sensor, the results are compared with conventional approach which presumed as without considering pyroelectric and pyromagnetic loads or in other words, the coefficients  $\gamma \neq 0$ ,  $p = 0$  and  $\tau = 0$ .

Table 1 Material properties of PZT5A and different volume fraction of multiphase magneto-electro-elastic BaTiO<sub>3</sub>-CoFe<sub>2</sub>O<sub>4</sub> (Aboudi 2001, Hadjiloizi *et al.* 2012, Chen *et al.* 2007, Biju *et al.* 2011)

	0.0v <sub>f</sub>	0.2v <sub>f</sub>	0.4v <sub>f</sub>	0.6v <sub>f</sub>	0.8v <sub>f</sub>	1.0v <sub>f</sub>	PZT-5A
Elastic constants							
c <sub>11</sub> =c <sub>22</sub>	286	250	225	200	175	166	99.2
c <sub>12</sub>	173	146	125	110	100	77	54
c <sub>13</sub> =c <sub>23</sub>	170	145	125	110	100	78	50.8
c <sub>33</sub>	269.5	240	220	190	170	162	86.9
c <sub>44</sub> =c <sub>55</sub>	45.3	45	45	45	50	43	21.1
Piezoelectric constants							
e <sub>31</sub> =e <sub>32</sub>	0	-2.0	-3.0	-3.5	-4.0	-4.4	-7.2
e <sub>33</sub>	0	4.0	7.0	11.0	14.0	18.6	15.1
e <sub>24</sub> =e <sub>15</sub>	0	0	0	0	0	11.6	12.3
Dielectric constants							
ε <sub>11</sub> =ε <sub>22</sub>	0.08	0.33	0.8	0.9	1.0	11.2	1.53
ε <sub>33</sub>	0.093	2.5	5.0	7.5	10.0	12.6	1.5
Magnetic permeability constants							
μ <sub>11</sub> =μ <sub>22</sub>	-5.9	-3.9	-2.5	-1.5	-0.8	0.05	0
μ <sub>33</sub>	1.57	1.33	1.0	0.75	0.5	0.1	0
Piezomagnetic constant							
q <sub>31</sub> =q <sub>32</sub>	580	410	300	200	100	0	0
q <sub>33</sub>	700	550	380	260	120	0	0
q <sub>24</sub> =q <sub>15</sub>	560	340	220	180	80	0	0
Magnetoelectric constants							
m <sub>11</sub> =m <sub>22</sub>	0	2.8	4.8	6.0	6.8	0	0
m <sub>33</sub>	0	2000	2750	2500	1500	0	0
Pyroelectric constants							
p <sub>2</sub>	0	-3.5	-6.5	-9	-10.8	0	
Pyromagnetic constants							
τ <sub>2</sub>	0	-36	-28	-18	-8.5	0	0
Thermal expansion coefficient							
β <sub>11</sub> =β <sub>22</sub>	10	10.8	11.8	12.9	14.1	15.7	1.5
β <sub>33</sub>	10	9.3	8.6	7.8	7.2	6.4	1.5
Density							
ρ	5300	5400	5500	5600	5700	5800	7750

c<sub>ij</sub> in N/m<sup>2</sup>, e<sub>ij</sub> in C/m<sup>2</sup>, ε<sub>ij</sub> in 10<sup>-9</sup>C<sup>2</sup>/N m<sup>2</sup> or 10<sup>-9</sup>C/V m, q<sub>ij</sub> in N/A m, μ<sub>ij</sub> in 10<sup>-4</sup>Ns<sup>2</sup>/C<sup>2</sup>, m<sub>ij</sub> in 10<sup>-12</sup>N s/V C, p<sub>i</sub> in 10<sup>-7</sup>C/m<sup>2</sup> K, τ<sub>i</sub> in 10<sup>-5</sup>C/m<sup>2</sup> K, β<sub>ij</sub> in 10<sup>-6</sup>1/K, ρ in kg/m<sup>3</sup>

### 3.1 Validation of the proposed formulation

A computer code has been developed to study the pyroelectric and pyromagnetic effects on the behavior of magneto-electro-elastic sensor bonded to mild steel cylindrical shell subjected to different boundary conditions. The arrangement consists of one electrode from the shell which is grounded and the other electrode which is kept on the top of the sensor patch.

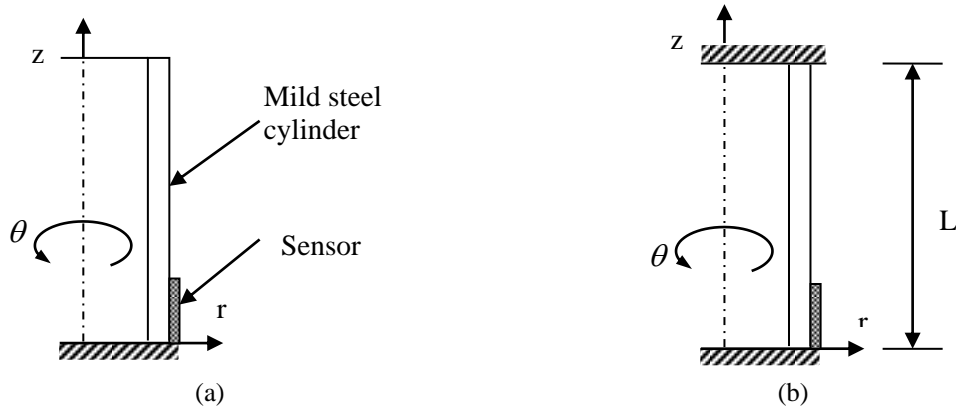
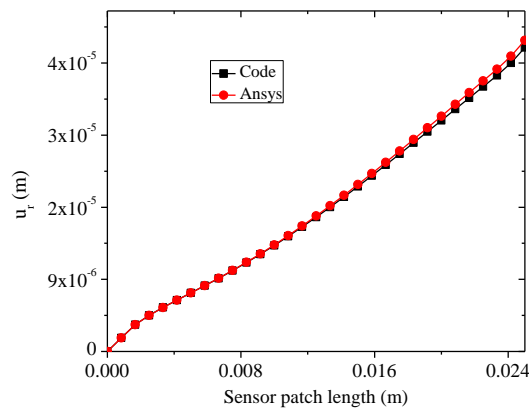
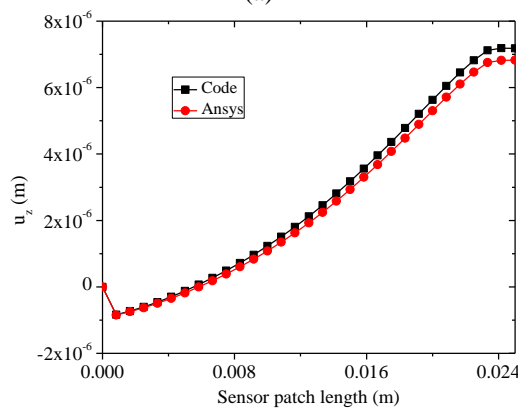


Fig. 1 Schematic diagram of mild steel cylinder with sensor bonded at an optimal location (clamped end) for (a) clamped-free and (b) clamped-clamped boundary conditions



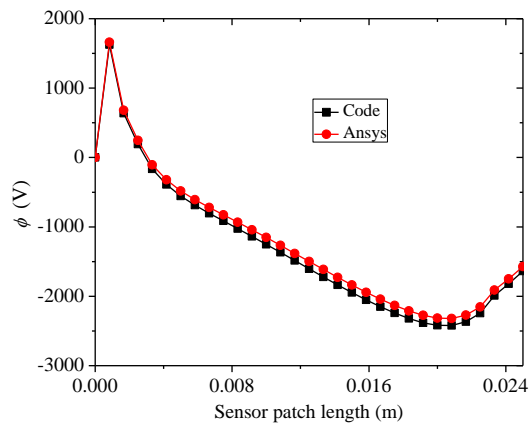
(a)



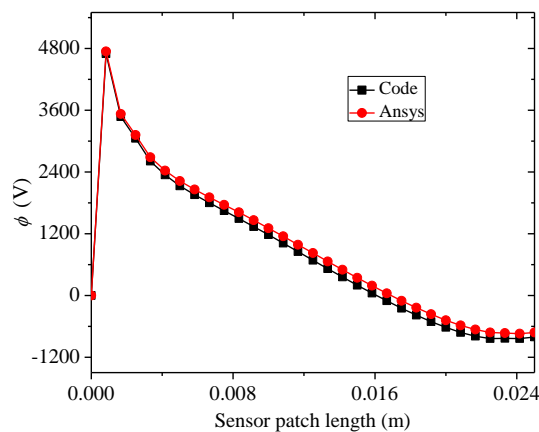
(b)

Fig. 2 Validation of (a) radial ( $u_r$ ) and (b) axial ( $u_z$ ) displacement components along the length on outer surface of the sensor patch (C-F boundary condition)

The piezomagnetic materials can be modeled using ANSYS since the constitutive relations as well as the governing field equations (if free currents and transient effects are neglected) are of identical format with piezoelectric materials. Since ANSYS does not explicitly contain piezomagnetic relationships, it is unable to model fully coupled MEE materials which involves the combined contributions of both piezoelectric and piezomagnetic material models. Thus commercial finite element package ANSYS was used for validating the methodology adopted for solution procedure. Hence the present code is validated using piezoelectric material PZT-5A whose material properties (Chen *et al.* 2007) are given in Table 1. Figs. 2 (a) and 2(b) shows the validation of radial ( $u_r$ ) and axial ( $u_z$ ) displacement components along the length on the top surface of piezoelectric sensor bonded to mild steel cylindrical shell under clamped-free boundary condition. Figs. 3(a) and 3(b) shows the validation of electric potential of the sensor along the length on outer surface of the sensor patch for clamped-free and clamped-clamped boundary conditions respectively. The results obtained by ANSYS are found to be in good agreement with the present formulation.



(a)



(b)

Fig. 3 Validation of electric potential along the length on outer surface of the sensor patch for (a) C-F and (b) C-C boundary conditions

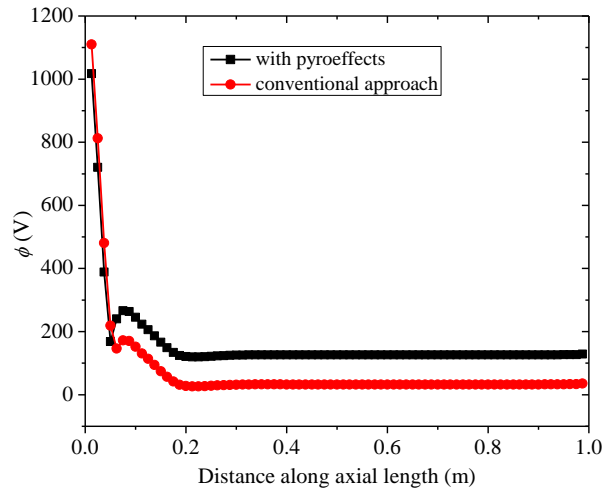


Fig. 4 Electric potential ( $\phi$ ) corresponding to the position of MEE sensor on outer surface of mild steel cylinder under clamped-free boundary condition

### 3.2 Optimal placement of MEE sensor

The optimal placement of MEE sensor on the outer surface of the mild steel cylindrical shell for obtaining maximum electric potential due to pyroeffects is studied. This study is carried out by implementing auto-mesh generation at different positions on outer surface along the length of the shell under clamped-free as well as clamped-clamped boundary conditions. It is assumed that the electric potential of the sensor is not arrested at clamped ends. Fig. 4 shows the electric potential ( $\phi$ ) corresponding to the position of the MEE sensor on outer surface along the length of the shell for clamped-free boundary condition. (Note: The effect on electric potential for clamped-clamped boundary condition is not shown in Figure, since the same trend as in for clamped-free boundary condition is observed). It is observed that the electric potential is maximum near the clamped end of the shell under both the boundary conditions. The pyroeffects on electric potential follows the same trend as in conventional approach. This optimal location of the sensor on outer surface of shell (clamped end) is considered to carry out the objective which discussed in Section 3 under both the boundary conditions.

### 3.3 Clamped-clamped boundary condition with sensor at optimal location

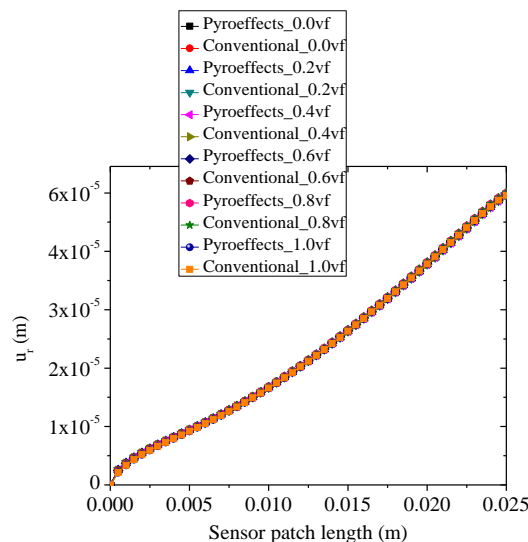
The pyroelectric and pyromagnetic effects on the behavior of multiphase magneto-electro-elastic sensor bonded on outer surface of cylindrical shell at the clamped end (optimal location) for uniform axisymmetric temperature under clamped-clamped boundary condition is studied. The study is carried out for different volume fractions of  $\text{BaTiO}_3$ . Figs. 5(a)-5(c) shows the variation of radial displacement component, electric and magnetic potentials on outer surface along the length of the sensor patch. (Note: The effect on axial displacement component is not shown in Figure, since the same trend as in radial displacement component is

observed). It is observed that the magnitude of radial displacement component is larger than the axial displacement component. There is no change in the magnitude of displacement components due to pyroelectric and pyromagnetic effects when compared to conventional approach.

The magnitude of electric potential is maximum near the clamped end and decreases along the length of the sensor for all volume fractions. The magnetic potential is oscillating continuously along the length of the sensor with different magnitudes for different volume fractions of the composite. The variation of electric and magnetic potentials with pyroeffects follows the same trend as the conventional approach. Unlike the displacement components, electric and magnetic potentials are affected by the pyroeffects. There is a decrease in electric potential and an increase in magnetic potential due to pyroeffects when compared to conventional approach. The pyroeffects on electric potential is maximum for volume fraction  $v_f = 0.2$  (Fig. 5(b)), and on magnetic potential, is maximum for volume fraction  $v_f = 0.4$ . (Fig. 5(c))

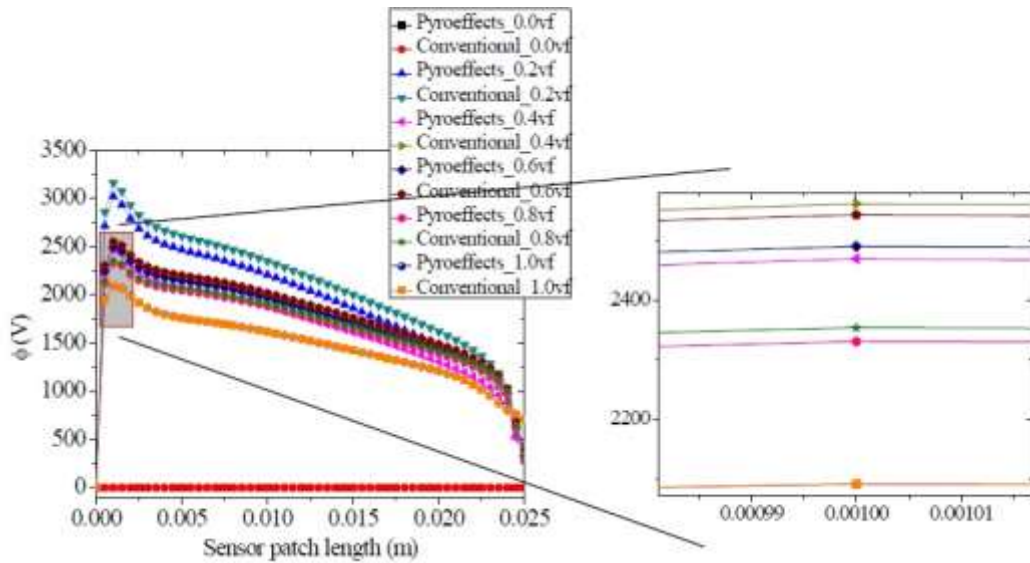
### 3.4 Clamped-free boundary condition with sensor at optimal location

The pyroeffects on behavior of multiphase MEE sensor bonded on the outer surface of cylindrical shell at clamped end (optimal location) for uniform axisymmetric temperature under clamped-free boundary condition is studied. Similar observations are noticed for displacement components in the clamped-free boundary condition as in case of clamped-clamped boundary condition. Hence the displacement components are not shown. Figs. 6(a) and 6(b) shows the variation of electric and magnetic potentials on outer surface along the length of the sensor patch. Similar observations are noticed in the clamped-clamped boundary condition as in case of clamped free boundary condition. The exception being the pyroeffects on electric potential is maximum in clamped-clamped boundary condition than clamped-free boundary condition when compared to conventional approach. The reason for lower magnitude maybe due to lower stress (clamped-free) when compared to the case where both sides of the shell are clamped.

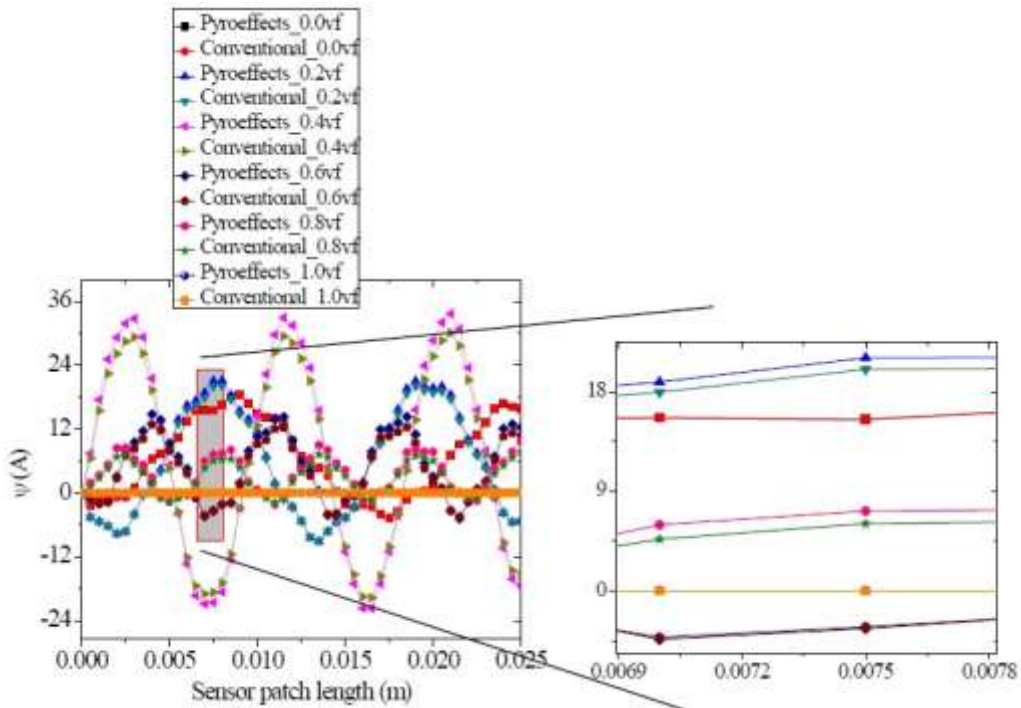


(a)

Continued

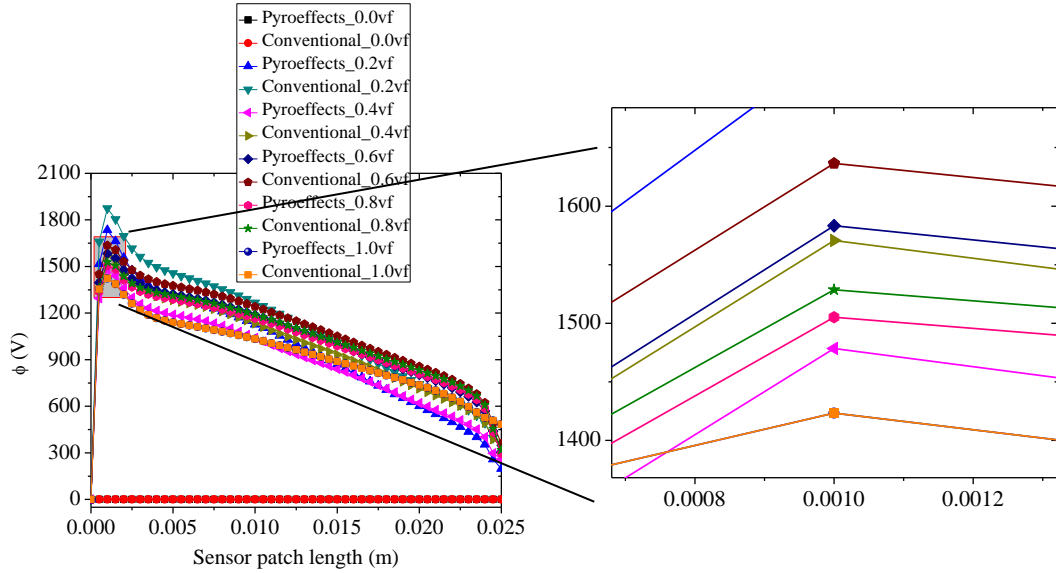


(b)

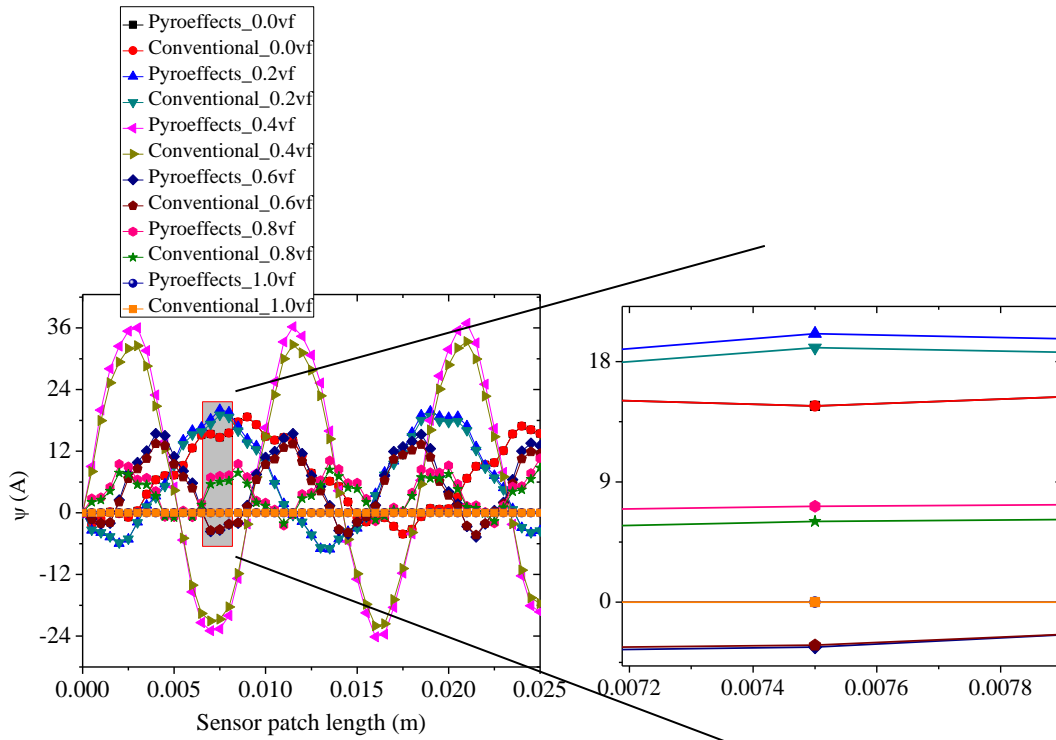


(c)

Fig. 5 Variation of (a) radial displacement component, (b) electric and (c) magnetic potentials with enlarged views along the length on outer surface of the sensor patch (C-C boundary conditions)



(a)



(b)

Fig. 6 Variation of (a) electric and (b) magnetic potentials with enlarged views along the length on outer surface of the sensor patch (C-F boundary conditions)

## 5. Conclusions

The pyroeffects on behavior of magneto-electro-elastic sensor bonded to mild steel cylinder is evaluated using semi-analytical finite element method. The pyroelectric and pyromagnetic loads which are generated from applied uniform axisymmetric temperature rise are used to study the pyroelectric and pyromagnetic effects to account for the thermal environment.

- It is seen that the radial and axial displacement components of the sensor patch are not affected by the pyroeffects.
- There is an increase in magnetic potential for increasing volume fraction of the composite due to pyroelectric and pyromagnetic effects under the both clamped-free as well as clamped-clamped boundary conditions.
- The pyroeffects on electric potential is maximum in the clamped-clamped boundary condition than clamped-free boundary condition when compared to conventional approach. The reason for lower magnitude maybe due to lower stress (clamped-free) when compared to the case where both the sides are clamped.
- The maximum pyroelectric and pyromagnetic effects on electric potentials is observed for volume fraction  $v_f = 0.2$  in both the boundary conditions. This can be attributed to the induced strain because of the high elastic constants for  $v_f = 0.2$ .

These studies will be very significant in enhancing the sensitivity of MEE sensor's electric and magnetic potentials in shell type structures subjected to uniform axisymmetric temperature rise.

## References

- Aboudi, J. (2001), "Micromechanical analysis of fully coupled electro-magneto-thermo-elastic multiphase composites", *Smart Mater. Struct.*, **10**(5), 867-877.
- Biju, B., Ganesan, N. and Shankar, K. (2011), "Dynamic response of multiphase magneto-electro-elastic sensors using 3D magnetic vector potential approach", *IEEE Sens. J.*, **11**(9), 2169 - 2176.
- Bravo-Castillero, J., Rodriguez-Ramos, R., Mechkour, H., Otero, J. and Sabina, F.J. (2008), "Homogenization of magneto-electro-elastic multilaminated materials", *Q. J. Mech. Appl. Math.*, **61**(3), 311-322.
- Chen, J., Pan, E. and Chen, H. (2007), "Wave propagation in magneto-electro-elastic multilayered plates", *Int. J. Solids Struct.*, **44**(3-4), 1073-1085.
- Daga A., Ganesan, N. and Shankar, K. (2009), "Behavior of magneto-electro-elastic sensors under transient mechanical loading", *Sensor Actuat. A - Phys.*, **150**(1), 46-55.
- Ganesan, N., Kumaravel, A. and Sethuraman, R. (2007), "Finite element modeling of a layered, multiphase magneto-electro-elastic cylinder subjected to an axisymmetric temperature distribution", *J. Mech. Mater. Struct.*, **2**(4), 655-674.
- Gao, C.F. and Noda, N. (2004), "Thermal-induced interfacial cracking on magneto-electro-elastic materials", *Int. J. Eng. Sci.*, **42**(13-14), 1347-1360.
- Guiffard, B., Zhang, J.W., Guyomar, D., Garbuio, L., Cottinet, P.J. and Belouadah, R. (2010), "Magnetic field sensing with a single piezoelectric ceramic disk: Experiments and modeling", *J. Appl. Phys.*, **108**(9), 094901.
- Hadjiloiizi, D.A., Georgiades, A.V., Kalamkarov, A.L. and Jothi, S. (2013a), "Micromechanical Modeling of Piezo-Magneto-Thermo-Elastic Composite Structures: Part I – Theory", *Eur. J. Mech. A. Solids*, **39**, 298-312.
- Hadjiloiizi, D.A., Georgiades, A.V., Kalamkarov, A.L. and Jothi, S. (2013b), "Micromechanical modeling of

- piezo-magneto-thermo-elastic composite structures: Part II – theory”, *Eur. J. Mech. A. Solids*, **39**, 313-327.
- Kalamkarov, A.L., Andrianov, I.V. and Vladyslav V., Danishevs’kyi (2009), “Asymptotic homogenization of composite materials and structures”, *Appl. Mech. Rev.*, **62**(3), 030802 (20pp).
- Kalamkarov, A.L. (2014), “Asymptotic homogenization method and micromechanical models for composite materials and thin-walled composite structures”, Chapter 1 in *Mathematical Methods and Models in Composites*, Imperial College Press, London.
- Mahieddine, A. and Quali, M. (2008), “Finite element formulation of a beam with piezoelectric patch”, *J. Eng. Appl. Sci.*, **3**, 803-807.
- Nan, C.W., Bichurin, M.I., Shuxiang D., Viehland, D. and Srinivasan, G. (2008), “Multiferroic magnetoelectric composites: Historical perspective, status, and future directions”, *J. Appl. Phys.*, **103**(3), 031101, 1-35.
- Ootao, Y. and Ishihara, M. (2011), “Exact solution of transient thermal stress problem of the multilayered magneto-electro-thermoelastic hollow cylinder”, *J. Solid Mech. Mater. Eng.*, **5**, 90-103.
- Pan, E. and Wang, R. (2009), “Effects of geometric size and mechanical boundary conditions on magnetoelectric coupling in multiferroic composites”, *J. Phys. D: Appl. Phys.*, **42**(24), 7, 245503.
- Ryu, J., Priya, S., Uchino, K. and Kim, H.E. (2002), “Magnetoelectric effect in composites of magnetostrictive and piezoelectric materials”, *J. Electroceram.*, **8**(2), 107-119.
- Sirohi, J. and Copra, I. (2000), “Fundamental understanding of piezoelectric strain sensors”, *J. Intel. Syst. Str.*, **11**(4), 246-257.
- Soh, A.K. and Liu, J.X. (2005), “On the constitutive equations of magneto-electroelastic solids”, *J. Intel. Mat. Syst. Str.*, **16**(7-8), 597-602.
- Sunar, M., Al-Garni, A.Z., Ali, M.H. and Kahraman, R. (2002), “Finite element modeling of thermopiezomagnetic smart structures”, *AIAA J.*, **40**(9), 1846-1851.
- Wu, T.L. and Huang, J.H. (2000), “Closed-form solutions for the magneto-electric coupling coefficients in Fibrous composites with piezoelectric and piezomagnetic phases”, *Int. J. Solids Struct.*, **37**(21), 2981-3009.